Leading and Trailing Edge Configuration for Distributed Electric Propulsion Systems

Mithun Eqbal, Matthew Marino, and Patrick Farley

Nomenclature

BLDC	Brushless direct current
BLI	Boundary layer ingestion
DA	Drag from the airframe
DEP	Distributed electric propulsion
ESC	Electronic speed control
GUI	Graphic user interface
I_R	Ingestion ratio
P_L	Power of the leading edge
P_T	Power of the trailing edge
P_{useful}	Useful power
PSC	Power saving coefficient
Re	Reynolds number
RPAS	Remotely piloted aircraft systems
T	Thrust
W	Watt
∂	Boundary layer length
u_J	Propeller airflow
u_w	Airframe drag
u_∞	Free stream velocity
u_1 and u_2	Airstream velocity
x	Length of the cross-section

M. Eqbal (✉) · M. Marino
RMIT University, Melbourne, Australia
e-mail: mithun.eqbal@rmit.edu.au; matthew.marino@rmit.edu.au

P. Farley
Deutsche Zentrum für Luft- und Raumfahrt e. V. (DLR), Weßling, Germany
e-mail: partick.farley@dlr.de

T. H. Karakoc et al. (eds.), *Green Approaches in Sustainable Aviation*, Sustainable Aviation, https://doi.org/10.1007/978-3-031-33118-3_15

1 Introduction

DEP (distributed electric propulsion) and BLI (boundary layer ingestion) provide a significant advantage on the aerodynamic efficiency of the aircraft (Davies et al., 2013; Hendricks, 2018; Plas et al., 2007; Rothhaar et al., 2014; Zhang et al., 2019). Studies were conducted, placing multiple propellers on leading-edge using advanced computational fluid dynamics (CFD). It is found that there are benefits like an increase in lift and reduction in drag; however, the advantages depend on the location of the propeller (Huang et al., 2018; Sinnige et al., 2019; Wang et al., 2018, 2019). Based on this, various leading-edge DEP concept prototypes are built and tested (Berg et al., 2015; Borer et al., 2016; Gohardani et al., 2011; Ko et al., 2003; Wang et al., 2018, 2019). Previous research has shown that a turbofan and boundary layer propulsion system on the wing's trailing edge capitalizes on BLI (Hall et al., 2017; Plas et al., 2007; Zhang et al., 2019) has demonstrated significant increases in propulsive efficiency. Combining both concepts proposes a new question: can an increase of propulsive efficiency be achieved by placing the propeller on the trailing edge of the wing to capitalize on the aerodynamic benefits of BLI? Few 2D CFD studies conducted similar comparisons and have shown improved propulsive efficiency but have created different losses in the process (El-Salamony & Teperin, 2017; Mantič-Lugo et al., 2013; Valencia et al., 2020). No conclusive wind tunnel or experimental studies have been conducted at this stage using propeller systems.

1.1 Theoretical Explanation

There is a connection between BLI and the benefits of the trailing edge, which leads to speed (Hall et al., 2017). The primary advantage of BLI is re-energizing the aircraft's wake, capitalizing on low-speed boundary layers, and enabling more efficient thrust when the flow is accelerated to generate propulsion (Tiseira Izaguirre et al., 2021). These two idealized solutions are shown in Fig. 1, where the flow is increased for a propeller situated in the front. As the flow traverses the top and bottom surfaces of the wing, a portion of its velocity is lost to frictional forces. This loss of velocity is transmitted to the surfaces of the wings and results in friction drag. This energy transfer is called energy recovery. Energy transmission and energy recovery are distinct for a propeller located on the wing's trailing edge. The wing is exposed to unbroken flow; however, when a boundary layer of flow builds across the surfaces, the momentum of the flow is diminished, similar to the preceding illustration. This boundary layer is composed of slower-moving flow; hence, when exposed to the propellor, it is propelled much faster than the surrounding flow, which travels at freestream velocity. As a result, boundary layer flow offers a mechanism for higher thrust. The slower flow is accelerated at more significant rates, therefore recovering a portion of the energy lost due to friction. This may be discussed in further detail using propulsion theory (Plas, 2006).

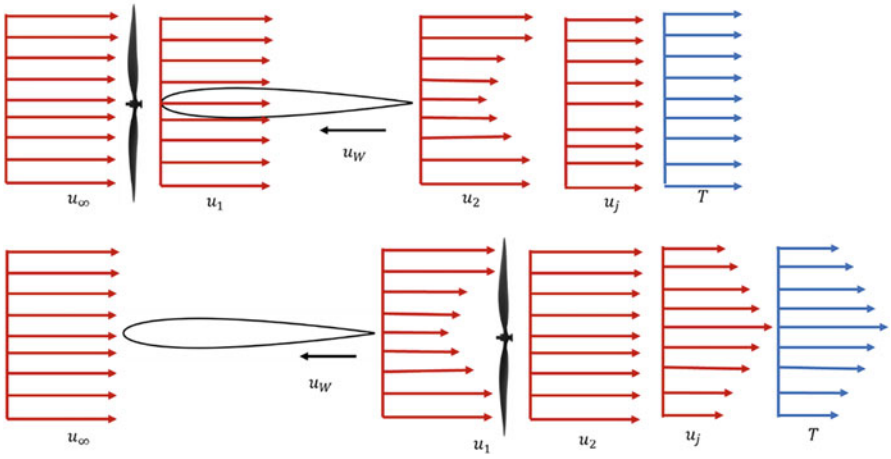

Fig. 1 Aerofoil with the leading edge and trailing edge with velocity

Where, u_∞ is the free stream velocity, u_J is the propeller air flow, T is the thrust, u_w is the airframe drag, u_1 and u_2 are airstream velocities through different phases.

Figure 1 shows that the flow is entering the propeller at freestream velocity (u_∞). The propeller accelerates the airflow to a velocity u_j, creating excess momentum to balance the momentum deficit (Plas, 2006). The momentum excess created by the propeller on the leading edge is equal to the momentum deficit of the airframe and is clearly defined by Plas (2006).

Due to the drag from the airframe D_A

$$T_p = m_*\left(u_j - u_\infty\right) = \frac{T}{2}\left(u_\infty - u_w\right) = D_A \tag{1}$$

The rate of mechanical energy added P_{Added} given to the flow by the propeller is provided by

$$P_{\text{Added},L} = \frac{m_*}{2}\left({u_j}^2 - {u_\infty}^2\right) = \frac{T}{2}\left(u_j + u_\infty\right) \tag{2}$$

The power required for the flight (P_{useful}) is given by

$$P_{\text{useful}} = D_A u_\infty = m_*(u - u_\infty)u_\infty \tag{3}$$

Suppose all the boundary layer is ingested and the propeller accelerates the wake back to freestream. The force provided by the propeller is

$$T_p = m_*\left(u_j - u_\infty\right) = m_*\left(u_\infty - u_w\right) = D_A \tag{4}$$

The rate of energy given to the flow by the propeller, $P_{\text{added, BLI,}}$ is

$$P_{\text{added},T} = \frac{m_*}{2}\left({u_j}^2 - {u_w}^2\right) = \frac{m_*}{2}\left({u_j}^2 - {u_\infty}^2\right) = \frac{F}{2}\left(u_w + u_\infty\right) \tag{5}$$

The power required for flight is the same as when the propeller is on the leading edge

$$P_{\text{useful}} = D_A u_\infty = m_*\left(u_j - u_\infty\right)u_\infty \tag{6}$$

Since $u_i > u_w$, comparison of Eqs. 4 and 5 shows,

$$P_{\text{added},L} > P_{\text{added},T} \tag{7}$$

It shows trailing edge needed less power to sustain the same drag on the airframe due to BLI.

This can be explained as follows: for a less specific force, less power needs to be added to a flow that enters the propeller with a lower velocity. Consider a flow that enters a propeller at velocity u_1 and exits at a velocity u_2. The thrust created by the propeller is:

$$T = m_*(u_2 - u_1) = m_*\Delta u \tag{8}$$

The power put to the flow is

$$P = \frac{m_*}{2}\left({u_2}^2 - {u_1}^2\right) = T\,\frac{u_1 + u_2}{2} = T\left(u_1 + \frac{\Delta_u}{2}\right) \tag{9}$$

For a constant mass flow and constant propulsive force, Δ_v is constant. A decrease in u_1 results in a decrease in power. That means for lower velocity, in the case of BLI fluid in trailing edge, less power input can create the same propulsive force.

To simplify, all this data can be written as power saving coefficient (PSC) as described by Blumenthal et al. (2019), Budziszewski and Friedrichs (2018), Gray et al. (2018) and Hall et al. (2017):

$$\text{PSC} = \frac{P_L - P_T}{P_L} \tag{10}$$

Where P_L is the leading edge and P_T is the trailing edge which has the direct influence on BLI.

Similarly thrust and power can be simplified as

$$T = m_*(u_{\text{out}} - u_{\text{in}}) = m_*(\Delta_u) \tag{11}$$

$$P = \frac{1}{2} m_* \left(u_{\text{out}}^2 - u_{\text{in}}^2\right) = \frac{1}{2} m_*(\Delta_u)) \tag{12}$$

In terms of propulsion efficiency, it can be defined as

$$n_p = \frac{u_\infty}{u_j + u_{in}} \tag{13}$$

2 Method

The wind tunnel used for the experiment is given in Fig. 2. It's a closed-circuit wind tunnel with a maximum speed of 140 km/h powered by a 380 kW DC motor. The tunnel has very low noise as it consists of anechoic turning vanes. Airflow can be changed using the speed controller located in the control room. The tunnel is equipped with an MKS differential pressure measuring system. The pitot static tube can be connected to calibrate the flow speed at different locations in the test section. The air temperature within the wind tunnel can be captured with the equipment provided.

An RC benchmark dynamometer 1520 (Benchmark, 2019) in Fig. 3 is used to measure the test power as it is designed for BLDC motor.

Fig. 2 Picture of the wind tunnel

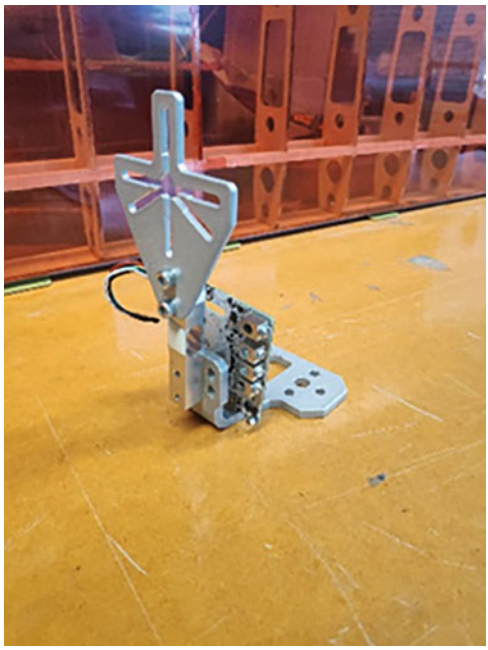

Fig. 3 RC benchmark mark dynamometer 1520

A constant supply power source is used to power the motor. The motor is controlled through electric speed control (ESC), where the ESC is throttled manually by using the graphics software interface (GUI) (Benchmark, 2019). An arbitrary velocity of 50 km/h is used to test the experiment. At the velocity of 50 km/h, the tip velocity of the propeller is under Mach 1, which is an essential consideration for the actuator disk theory so that the results can be verified without anomalies. Similarly, there is no propeller interference. If the interaction is there, the results need to consider aerodynamics and power integration, which are of future interest. Also, it needs more power and propeller integration factors, which gives a higher margin of error. Additionally, the test is only done for a zero angle of attack to reduce the complexities associated, but one angle of attack is enough to prove the test result (Stoll et al., 2014).

A brushless direct current (BLDC) 1650 KV motor as in Table 1 and three propeller configurations as given in Table 2 are studied to effectively determine the area's impact on power, thrust, and propulsive efficiency.

The propeller arrangement is given in Figs. 4 and 5. The trailing edge propeller is arranged not on the edge of the wing but close enough to conceal the motor inside the wing to avoid extra drag for the arrangement, more explanation is given in Sect. 3.

Table 1 Details of the BLDC motor and ESC used for testing

Parameters	Number
Dimension (motor)	28 mm × 25 mm
Weight	49 g
KV	1650 rpm/V
Voltage	7.2 v ~ 11.1 v (2 s ~ 3 s)
Max power Max current	180 W 17.5 A
Dimension (ESC)	30 × 17.5 × 10 mm
Weight	14.5 g
Voltage	2 ~ 4 S (8.4 ~ 16.8 V)
Max current	20 A

Table 2 Details of the propeller used for testing

Propeller	Type and specifications	Brand
7x6	2 blade plastic with 0.50 inch hub diameter, 0.32 hub thickness, ¼ inch shaft diameter and 0.18 oz weight	APC 7x6 slow flyer propeller
8x6	2 blade plastic with 0.50 inch hub diameter, 0.30 inch hub thickness, ¼ inch shaft diameter, and 0.25 oz weight	APC 8x6 slow fly propeller
9x6	2 blade plastic with 0.50 inch hub diameter, 0.30 inch hub thickness, ¼ inch shaft diameter, and 0.32 oz weight.	APC 9x6 slow fly propeller

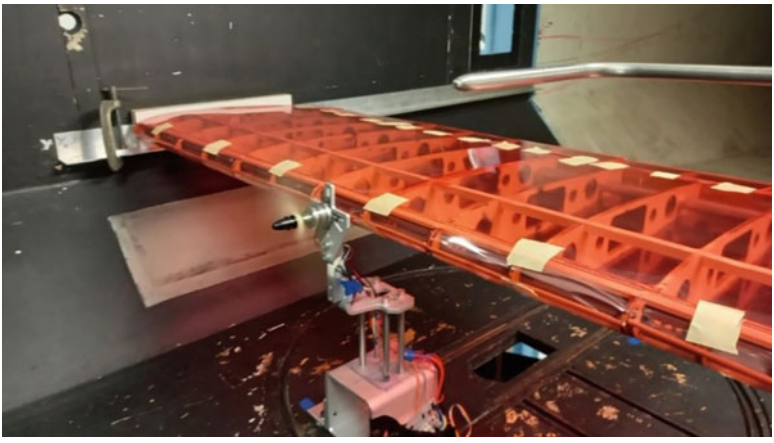

Fig. 4 Wind tunnel testing setup for a leading-edge test

2.1 Calculation of Power Saving Coefficient and Ingestion Ratio

The explanation of power saving is defined in Eq. 10 (Gray et al., 2018) as an effect of BLI. A thrust setting is chosen to explain the power saving coefficient at a specific point. Similarly, the effective area of the propeller can be defined in the trailing edge

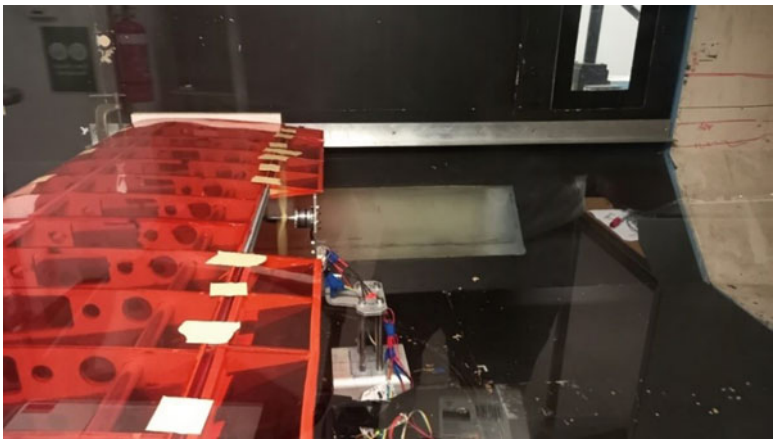

Fig. 5 Wind tunnel testing setup for a trailing-edge test

Fig. 6 Boundary layer

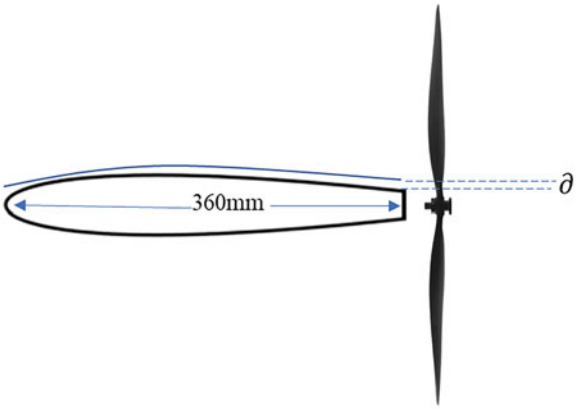

arrangement. Figure 6 gives a cross-section representation of the aerofoil used for the experiment and propeller.

A typical UAS flight occurs at low Reynolds Numbers and within the atmospheric boundary layer. This flight regime increases the probability of a turbulent boundary layer formation. A turbulent boundary layer model is assumed and is likely to produce a conservative estimate of the growth of the boundary layer for a typical UAS flight. From Itoh et al. (2005), the length of the boundary layer can be explained by Eq. (14)

$$\partial = \frac{0.37x}{\mathrm{Re}^{0.2}} \tag{14}$$

Where, ∂ is the boundary layer length, x is the length of the cross section, where this is chord length and Re is the Reynolds number, where it is defined as

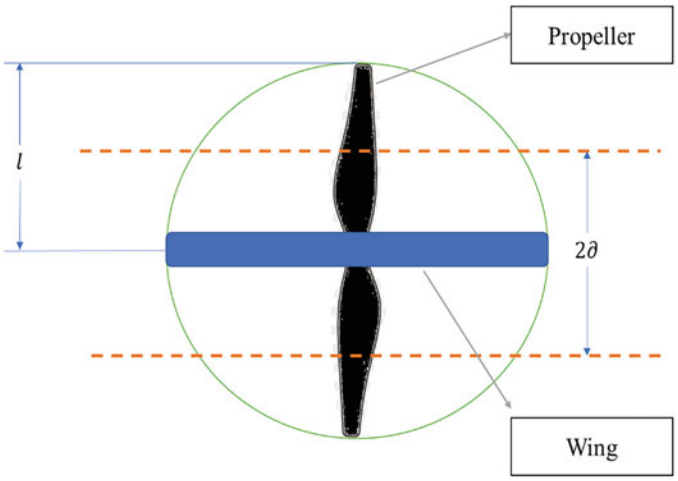

Fig. 7 Area of propeller relative to wing

$$\mathrm{Re} = \frac{\rho\, u\, L}{\mu} \tag{15}$$

From Eq. (15), the boundary layer can be calculated, and the length of the propeller is known from the manufacturers data (Table 2).

As given in Fig. 7 and with known data, the area of propeller and the boundary layer can be calculated. This is defined as ingestion ratio (I_R).

$$I_R = \frac{\text{Areaof the Boundary layer}}{\text{Area of the Propeller}} \tag{16}$$

From Eqs. 10, 11, 12, 13, 14, 15, and 16, the factors power saving coefficient (PSC) and ingestion ratio (I_R) are defined. These equations form a base to explain the performance of the experimental analysis or leading and trailing edge. The drag created by the leading edge and trailing edge is different, which needs an explanation not to add more drag to the arrangement.

3 Drag Estimation and Motor Arrangement

One of the significant factors to consider is whether the installation arrangement needed for anchoring the motor on the trailing edge can create additional drag and overrun the gains made by trailing edge propulsive efficiency. However, this can be easily solved by designing the installation mount, as in Fig. 8.

Figure 8 shows the dimension of the aerofoil used for the testing and the electric motor's measurement. The length of the aerofoil near the trailing edge at the

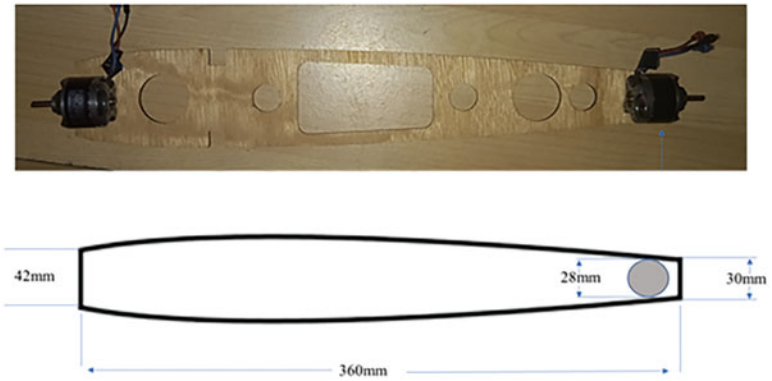

Fig. 8 Aerofoil and motor arrangement

outermost tip is 30 mm, while the diameter of the motor is 28 mm. So, the motor can be easily concealed inside the aerofoil to avoid drag from the installation with some proper mount design. The experimental testing of the drag is for future work where the aerofoil coupled to the motor will be tested in the wind tunnel.

Previously, Junzi described the use of the drag estimation in open aerodynamic model, where he deliberately avoided utilizing manufacturer data (unless they are freely accessible) and looked for another method to estimate the drag, i.e., the actual energy model often represents energy change by multiplying every force by the corresponding direction's speed.

4 Results and Discussion

In this section, the experiment results are discussed in more detail. The issue is simplified by reflecting on the assumptions that were made in an attempt to make it more manageable. Finally, we also discuss the restrictions and ambiguities of the offered approaches. This study aims to investigate the impact on power savings and advancements in propellant efficiency that would result from mounting the propeller on the trailing edge of the wing rather than the leading edge of the wing. Using a brushless direct current (BLDC) engine and various propeller configurations, a scaled-down remotely piloted aircraft systems (RPAS) wing is put through its paces in a wind tunnel. The impact that the change in propeller size has on the amount of electricity that may be saved is referred to as the ingestion ratio (IR), which is a brand new word. The PSC is connected to the reduced intake velocity of the trailing edge, which helps to boost the propulsive efficiency of the trailing arrangement efficiently. It is essential to have a solid understanding that every parameter is treated as a random variable (described by probability density functions) in the hierarchical model that has been provided. Testing uses almost all of the

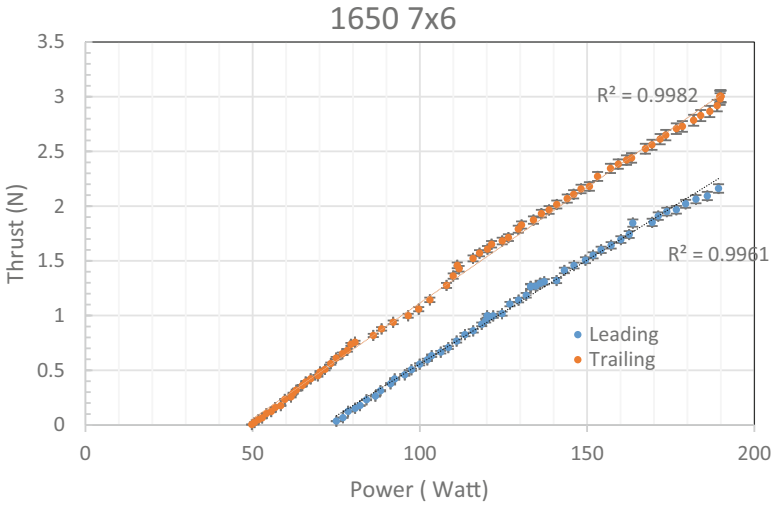

Fig. 9 Thrust by power for a 7x6 propeller configuration

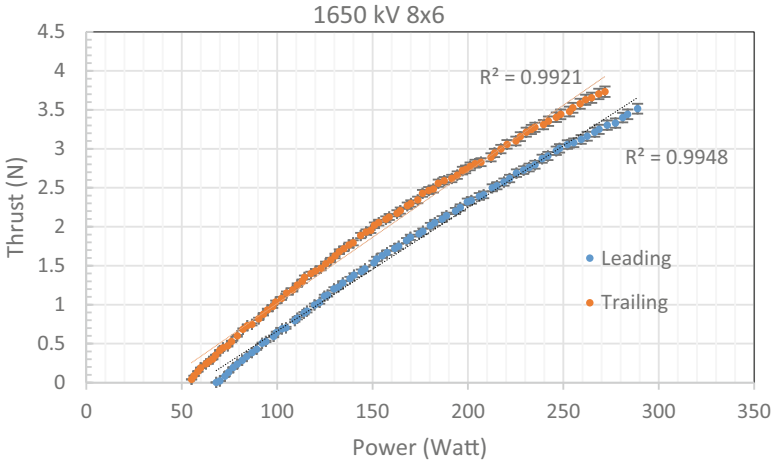

Fig. 10 Thrust by power for an 8x6 propeller configuration

settings of the BLDC motor and the ESC. The tests conducted with various propeller configurations were represented as multi-dimensional probability density functions.

In addition, there is a downward tendency in the PSC when there is a rise in the propeller's surface area. This helps to explain why the ingestion ratio offered by the smaller wing area is more significant than that provided by the larger wing area since the boundary layer directly affects the smaller wing area.

The experiment results for the 7x6, 8x6, and 9x6 for the 50 km/h wind setting are given in Figs. 9, 10, and 11, respectively.

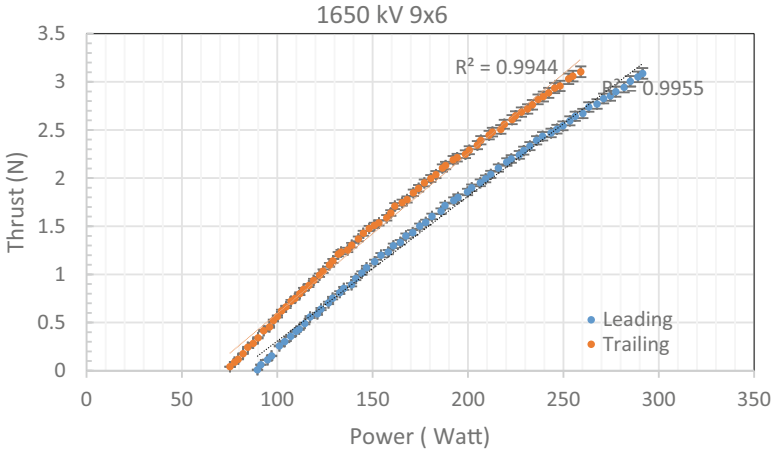

Fig. 11 Thrust by power for a 9x6 propeller configuration

Table 3 Summary of the test results for the test with different propeller configuration

Propeller type for thrust 1.6–1.8 N	Ingestion ratio	PSC	Power savings (W)	Propulsive efficiency savings
7x6	7.02	0.22	33.98	5.80
8x6	5.37	0.15	29.36	3.82
9x6	4.32	0.13	24.70	2.81

In all the cases, the thrust and power didn't start from zero. This is because of electrical losses, idle power as well as the thrust stand only starts recording at a specific thrust to overcome the drag associated with the flowing wind.

Figures 9, 10, and 11 show a decrease in power consumption when the propeller is placed on the trailing edge throughout the throttle setting. An effective reduction in power consumption is evident. Now using the Eqs. 13, 14, 15, and 16, the ingestion ratio, PSC, power savings, and propulsive efficiency are calculated from the experiment for a thrust setting between 1.6 and 1.8 N and are tabulated in Table 3.

As explained in Eq. 10, the PSC is related to the lower inlet velocity for the trailing edge and effectively increases the propulsive efficiency for the trailing arrangement. Also, there is a reducing trend in the PSC with increase in propeller area. This explains the ingestion ratio provides a higher the ingestion ratio provided by the smaller wing area, which is directly affected by the boundary layer.

5 Conclusion

The experiment demonstrated that mounting the propeller on the trailing edge of the wing results in greater propulsive efficiency and a reduction in the amount of power used by taking advantage of BLI. This has significant repercussions for aircraft that use distributed electric propulsion. It is validated on various BLDC motor and propeller combinations using wind tunnel testing at a predetermined speed. A new factor ingestion ratio has been created to describe the effect ratio of boundary layer and propeller area on trailing edge efficiency. For a single motor propeller arrangement, the ingestion ratio may contribute to a power savings of 24.7% and propulsive efficiency of 5.8%. The higher the ingestion ratio, the more significant the improvement in propulsive efficiency and power savings.

Acknowledgment We would like to acknowledge Mr. Singh for his proof reading and editing support.

References

Benchmark, R. (2019). https://cdn-docs.rcbenchmark.com/datasheets/series-1520/Datasheet-RCbenchmark-Series-1520.pdf

Berg, F., Palmer, J., Miller, P., Husband, M., & Dodds, G. (2015). HTS electrical system for a distributed propulsion aircraft. *IEEE Transactions on Applied Superconductivity, 25*(3), 1–5.

Blumenthal, B. T., Elmiligui, A. A., Geiselhart, K. A., Campbell, R. L., Maughmer, M. D., & Schmitz, S. (2019). Computational investigation of a boundary-layer ingesting propulsion system for the common research model. *Journal of Aircraft, 55*(3), 1141–1153.

Borer, N. K., Patterson, M. D., Viken, J. K., Moore, M. D., Bevirt, J., Stoll, A. M., & Gibson, A. R. (2016). Design and performance of the NASA SCEPTOR distributed electric propulsion flight demonstrator. In *16th AIAA aviation technology, integration, and operations conference* (p. 3920).

Budziszewski, N., & Friedrichs, J. (2018). Modelling of a boundary layer ingesting propulsor. *Energies (Basel), 11*(4), 708.

Davies, K., Norman, P., Jones, C., Galloway, S., & Husband, M. (2013). *A review of turboelectric distributed propulsion technologies for N+ 3 aircraft electrical systems* (pp. 1–5). IEEE.

El-Salamony, M., & Teperin, L. (2017). 2D numerical investigation of boundary layer ingestion propulsor on Airfoil. In *7th European conference for aeronautics and aerospace sciences*, Milan, Italy.

Gohardani, A. S., Doulgeris, G., & Singh, R. (2011). Challenges of future aircraft propulsion: A review of distributed propulsion technology and its potential application for all electric commercial aircraft. *Progress in Aerospace Sciences, 47*(5), 369–391.

Gray, J. S., Mader, C. A., Kenway, G. K. W., & Martins, J. R. R. A. (2018). Modeling boundary layer ingestion using a coupled aeropropulsive analysis. *Journal of Aircraft, 55*(3), 1191–1199.

Hall, D. K., Huang, A. C., Uranga, A., Greitzer, E. M., Drela, M., & Sato, S. (2017). Boundary layer ingestion propulsion benefit for transport aircraft. *Journal of Propulsion and Power, 33*(5), 1118–1129.

Hendricks, E. S. (2018). *A review of boundary layer ingestion modeling approaches for use in conceptual design*. NASA Glenn Research Center.

Huang, X., Zhao, X., & Huang, J. (2018). A simplified model for predicting the propeller-wing interaction. *Aircraft Engineering and Aerospace Technology, 90*(1), 196–201.

Itoh, M., Tamano, S., Yokota, K., & Ninagawa, M. (2005). Velocity measurement in turbulent boundary layer of drag-reducing surfactant solution. *Physics of Fluids (1994), 17*(7), 1–9.

Ko, A., Schetz, J., & Mason, W. (2003). Assessment of the potential advantages of distributed propulsion for aircraft. In *XVI international symposium on air breathing engines*, Cleveland, Ohio.

Mantič-Lugo, V., Doulgeris, G., & Singh, R. (2013). Computational analysis of the effects of a boundary layer ingesting propulsion system in transonic flow. *Proceedings of the Institution of Mechanical Engineers, Part G: Journal of Aerospace Engineering, 227*(8), 1215–1232.

Plas, A. (2006). *Performance of a boundary layer ingesting propulsion system*. Master of Science thesis, Massachusetts Institute of Technology. https://dspace.mit.edu/handle/1721.1/35568

Plas, A., Crichton, D., Sargeant, M., Hynes, T., Greitzer, E., Hall, C., & Madani, V. (2007, January). Performance of a boundary layer ingesting (BLI) propulsion system. In *AIAA 2007–450. 45th AIAA aerospace sciences meeting and exhibit*.

Rothhaar, P. M., Murphy, P. C., Bacon, B. J., Gregory, I. M., Grauer, J. A., Busan, R. C., & Croom, M. A. (2014). NASA Langley distributed propulsion VTOL tiltwing aircraft testing, modeling, simulation, control, and flight test development. In *14th AIAA aviation technology, integration, and operations conference* (p. 2999).

Sinnige, T., Stokkermans, T. C. A., Arnhem, N., & Veldhuis, L. L. M. (2019). Aerodynamic performance of a wingtip-mounted tractor propeller configuration in windmilling and energy-harvesting conditions. In *AIAA aviation 2019 forum* (p. 1624105890).

Stoll, A. M., Bevirt, J., Moore, M. D., Fredericks, W. J., & Borer, N. K. (2014). Drag reduction through distributed electric propulsion. In *Aviation technology, integration, and operations conference*, 16–20 June 2014, Atlanta, Georgia.

Tiseira Izaguirre, A. O., García-Cuevas González, L. M., Quintero Igeño, P., & Varela Martínez, P. (2021). Series-hybridisation, distributed electric propulsion and boundary layer ingestion in long-endurance, small remotely piloted aircraft: Fuel consumption improvements. *Aerospace Science and Technology, 2021*, 107227.

Valencia, E., Alulema, V., Rodriguez, D., Laskaridis, P., & Roumeliotis, I. (2020). Novel fan configuration for distributed propulsion systems with boundary layer ingestion on an hybrid wing body airframe. *Thermal Science and Engineering Progress, 18*, 100515. ISSN 2451-9049.

Wang, H., Zhou, Z., Xu, X., & Zhu, X. (2018). Influence analysis of propeller location parameters on wings using a panel/viscous vortex particle hybrid method. *The Aeronautical Journal, 122*(1247), 21–41.

Wang, K., Zhou, Z., Zhu, X., & Xu, X. (2019). Aerodynamic design of multi-propeller/wing integration at low Reynolds numbers. *Aerospace Science and Technology, 84*, 1–17.

Zhang, J., Kang, W., & Yang, L. (2019). Aerodynamic benefits of boundary layer ingestion for distributed propulsion configuration. *Aircraft Engineering and Aerospace Technology, 91*(10), 1285–1294.